

Classification of Interstitial lung disease patterns in CT images using convolutional neural network

Jenu J¹, Ajith Kumar D²

*1P.G Scholar, Dept. of Biomedical Engineering
Udaya School of Engineering, Vellamodi, Tamil Nadu, India*

*2 Asst. Professor, Dept. of Biomedical Engineering,
Udaya School of Engineering, Vellamodi, Tamil Nadu, India*

Abstract-Automated tissue characterization is one of the most crucial components of a computer aided diagnosis (CAD) system for interstitial lung diseases (ILDs). Although much research has been conducted in this field, the problem remains challenging. Deep learning techniques have recently achieved impressive results in a variety of computer vision problems, raising expectations that they might be applied in other domains, such as medical image analysis. In this paper, we propose and evaluate a convolutional neural network (CNN), designed for the classification of ILD patterns. The proposed network consists of 5 convolutional layers with 2x2 kernels and LeakyReLU activations, followed by average pooling with size equal to the size of the final feature maps and three dense layers. The last dense layer has 7 outputs, equivalent to the classes considered: healthy, ground glass opacity (GGO), micro nodules, consolidation, reticulation, honeycombing and a combination of GGO/reticulation. To train and evaluate the CNN, we used a dataset of 1469 image patches, derived by 20 CT scans from different scanners and hospitals. To the best of our knowledge, this is the first deep CNN designed for the specific problem. The classification performance demonstrated the potential of CNNs in analysing lung patterns.

Key Words: Micro nodules, honeycombing, image analysis, classification

1.1 OVERVIEW

The term interstitial lung disease (ILD) refers to a group of more than 200 chronic lung disorders characterized by inflammation of the lung tissue, which often leads to scarring usually referred to as pulmonary fibrosis. Fibrosis may progressively cause lung stiffness, reducing the ability of the air sacs to capture and carry oxygen into the bloodstream and eventually leads to permanent loss of the ability to breathe. ILDs accounts for 15 percent of all cases seen by pulmonologists and can be caused by autoimmune diseases, genetic abnormalities and long-term exposures to hazardous

materials. However, the cause of ILDs is mostly unknown and the lung manifestations are described as idiopathic interstitial pneumonia (IIP). In 2002, an international multidisciplinary consensus conference, including the American Thoracic Society (ATS) and the European Respiratory Society (ERS), proposed a classification for ILDs in order to establish a uniform set of definitions and criteria for their diagnosis.

Patients also have different physical conditions and medical histories; hence even those with the same type of ILD could display quite different tissue patterns. As a consequence, manual interpretation of the images could be error prone, especially when the radiologists are under heavy workload with short time frames. It is thus suggested that an automatic system for differentiating the tissue patterns would be useful to provide initial screening or second opinions

The diagnosis of an ILD involves questioning the patient about their clinical history, a thorough physical examination, pulmonary function testing, a chest X-ray and a CT scan. High resolution computed tomography (HRCT) is generally considered to be the most appropriate protocol, due to the specific radiation attenuation properties of the lung tissue. The imaging data are interpreted by assessing the extent and distribution of the various ILD textural patterns in the lung CT scan. Typical ILD patterns in CT images are: reticulation, honeycombing, ground glass opacity (GGO), consolidation and micro nodules.

However, in some cases, the diagnosis cannot be confirmed radiologically. Although ILDs are a histologically heterogeneous group of diseases, they mostly have rather similar clinical manifestations with each other, or even with different lung disorders, so that differential diagnosis is fairly difficult even for experienced physicians. This inherent property of ILDs, as well as the lack of strict clinical guidelines and the large

quantity of radiological data that radiologists have to scrutinize, explains the low diagnostic accuracy and the high inter- and intra- observer variability, which has been reported to be as great as 50%. In ambiguous cases, additional invasive procedures are required, such as Broncho alveolar lavage and histological confirmation. However, performing a surgical biopsy exposes the patient to a number of risks and increases the healthcare costs, while even such methods do not always provide a reliable diagnosis.

To avoid the dangerous histological biopsies, much research has been conducted on computer aided diagnosis systems (CAD) which could assist radiologists and increase their diagnostic accuracy. A CAD system for lung CT scan assessment typically consists of three stages: (a) lung segmentation, (b) lung disease quantification and (c) differential diagnosis. The first stage refers to the identification of the lung border, the separation of the lobes and in some cases the detection and removal of the Broncho vascular tree. The second stage includes detection and recognition of the different tissue abnormalities and estimation of their extent in the lung. Finally, the third stage combines the previous results to suggest a probable differential diagnosis. This study focused on the second stage and especially on the classification of lung tissue with different ILD abnormalities. Image classification is normally performed in two stages: feature extraction for encoding the image features as feature descriptors, and labelling of image categories using supervised approaches. Being an active research field for a long time, most of the image classification techniques have been applied to a wide range of imaging problems, including the lung CT images. Mainly the recent works on lung CT images to cover the popular methodologies, and only include studies from other imaging domains if the proposed methods are not normally used for lung studies.

A basic understanding of pulmonary anatomy is required for accurate HRCT interpretation. Pulmonary anatomy may be broadly divided into the pulmonary gas exchange units and the pulmonary interstitium. The pulmonary interstitium may be further subdivided into the central peribroncho vascular interstitium and the peripheral centrilobular interstitium; these two fibre networks are continuous with one another. The central peribronchovascular interstitium invests the larger central bronchi and vessels near the pulmonary hilum and courses peripherally, producing the peripheral centrilobular interstitium, eventually merging with the sub pleural interstitial fibre network. The latter is located immediately beneath the visceral pleura and extends into the underlying lung parenchyma at various intervals to produce interlobular septa.

1.1.1 Interstitial Lung Diseases patterns

1.1.1.1 Micro nodules

A pulmonary nodule may be broadly defined as any relatively sharply defined, discrete, nearly circular opacity within the lung, ranging in size from 2 to 30 mm. Nodules are usually further characterized with respect to size, border

definition, density, number, and location. The term “micro nodule” is occasionally used when describing HRCT findings, usually referring to nodules less than 3 to 7 mm in size, as shown in fig. 1.1. But the significance of this designation is uncertain.

The diagnostic value of HRCT for the assessment of diffuse nodular diseases relies heavily on the distribution of the nodules relative to the secondary pulmonary lobule, a diagnostic approach that was first recognized as valuable for interpretation of biopsy and surgical histopathologic specimens. HRCT technique allows imagers to extrapolate these pathologic findings to imaging findings.

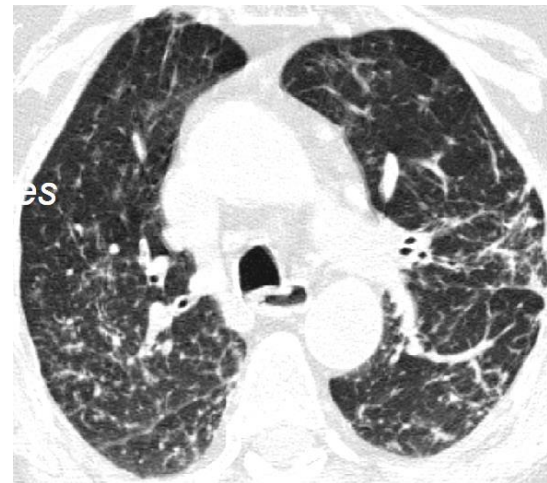


Fig 1.1 Micro nodules on HRCT imaging

1.1.1.2 Ground-glass opacity

Ground-glass opacity is defined as hazy increased attenuation that does not obscure visibility of the underlying vasculature. Ground-glass opacity is a nonspecific finding that may reflect volume averaging of abnormalities that cannot be completely resolved with HRCT technique, a purely interstitial abnormality, a purely alveolar abnormality, or a disease process that involves both the pulmonary interstitium and the air spaces. The histopathologic correlates of ground-glass opacity on HRCT showed that 54% of patients had a primarily interstitial abnormality, 32% had a mixed interstitial and alveolar process, and 14% of patients had primarily an alveolar process. The fig 1.2 shows the Ground-glass opacity.

The significance of ground-glass opacity depends on the patient's symptoms (acute versus chronic, and the actual presenting symptoms); the distribution of the ground-glass opacity on HRCT; and the presence or absence of other findings on the HRCT study. In severely immunocompromised patients with a clinical presentation suggesting

infection, ground-glass opacity often reflects active infection. In patients presenting with haemoptysis, falling haematocrit, or pulmonary capillary's, multifocal ground glass opacity often reflects pulmonary haemorrhage. For patients with a suggestive antigen exposure, multifocal ground-glass opacity reflects the histopathologic presence of poorly formed granulomas, cellular bronchiolitis, and interstitial inflammation caused by hypersensitivity pneumonitis. The presence of ground-glass opacity in patients with idiopathic interstitial pneumonias often, but not invariably, reflects active pulmonary inflammation and potentially reversible disease.

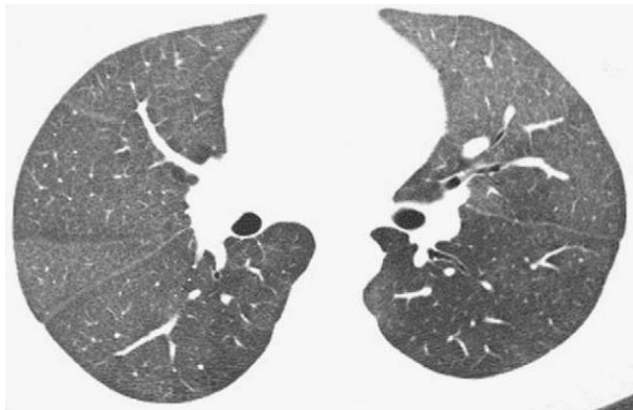


Fig 1.2 Ground-glass opacity on HRCT imaging

1.1.1.3 Consolidation

Consolidation is defined as increased attenuation, which results in obscuration of the underlying vasculature, usually producing air bronchogram., as shown in fig 1.3. The presence of consolidation implies that the air within affected alveoli has been replaced by another substance, such as blood, pus, edema, or cells. When consolidation is evident on a chest radiograph, HRCT does not usually provide additional diagnostically useful information. HRCT may detect consolidation earlier than chest radiography, however, and in certain circumstances may provide useful information regarding the distribution of consolidation and detect findings diagnostically important but not visible radiographically.

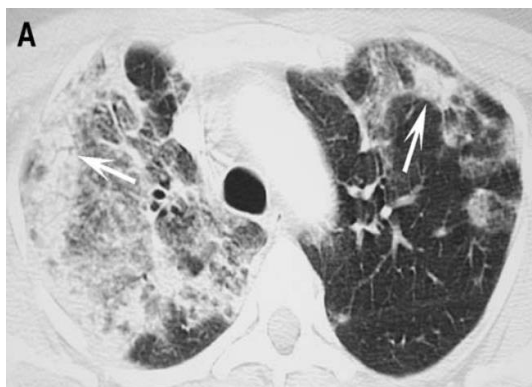


Fig 1.3 Consolidation on HRCT imaging

The differential diagnosis of consolidation is extensive, and requires integration of clinical history with other relevant scan findings to become manageable. One circumstance where HRCT is quite valuable in the assessment of consolidation is the determination of the distribution of findings. Although many etiologies of consolidation may often be indistinguishable from one another on HRCT imaging, consolidation in a peripheral or subpleural distribution should evoke a specific differential diagnosis. Recognition of this particular distribution of consolidation can be diagnostically quite useful.

1.1.1.4 Honeycombing

The fig 1.4 shows the Honeycomb lung that represents the presence of end-stage lung and may occur from a wide variety of insults. Pathologically, honeycomb cysts consist of air-containing spaces with thick walls that are lined with bronchiolar epithelium and fibrous tissue. The HRCT demonstration of honeycomb cysts allows for a confident diagnosis of a fibro pulmonary process, and the specific distribution of the honeycomb cysts may be a clue to the etiologic of the fibrotic lung disease. Note, however, that microscopic honeycomb cysts may be shown on surgical lung biopsy in patients without clear evidence of honeycomb cysts on HRCT.

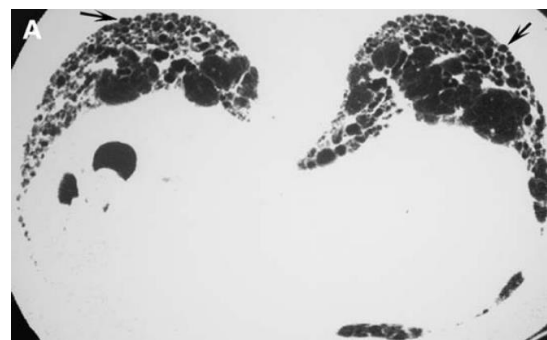


Fig 1.4 HRCT demonstration of honeycombing

Honeycomb cysts on HRCT appear as cystic areas with clearly definable walls, ranging from a few millimetres to several centimetres in size. Honeycomb cysts may form a single layer in the sub pleural lung, although when the disease process becomes more advanced, honeycomb cysts stack on one another in several layers this allows them to be readily distinguished from bullae in patients with Para septal emphysema. Honeycomb cysts usually share walls with one another, and associated findings of fibrosis (architectural distortion, coarse reticulation, interlobular

interstitial thickening, and traction bronchiectasis) are also commonly present the determination of the presence or absence of honeycombing on HRCT in patients with idiopathic interstitial pneumonia is of great importance.

The confident diagnosis of lower lobe, subpleural honeycombing in such patients strongly suggests usual interstitial pneumonia–idiopathic pulmonary fibrosis and obviates the need for surgical lung biopsy. In a group of patients from multiple centers selected on the basis of the suspicion of idiopathic pulmonary fibrosis, thoracic radiologists confidently diagnosed usual interstitial pneumonia in nearly 60% of patients, with a positive predictive value of 96%. In a subsequent analysis of these data, the presence of either of two HRCT features (upper lobe reticulation and lower lobe honeycombing) was found to increase the probability of a histopathologic diagnosis of usual interstitial pneumonia by fivefold to six fold. Similarly, in another study of patients suspected of having an idiopathic interstitial pneumonia, the presence of honeycombing on HRCT in at least one lobe had a positive predictive value of 92%. The diagnosis of usual interstitial pneumonia cannot be confidently offered on HRCT imaging when honeycomb cysts are not seen. Some patients without HRCT evidence of honeycombing subsequently have usual interstitial pneumonia diagnosed on surgical lung biopsy.

1.1.1.5 Reticulation

Reticular opacities represent linear opacities that intersect one another at various angles, producing a netlike pattern, shown in fig 1.5. The most important form of reticular opacity encountered on HRCT imaging is interlobular interstitial thickening. Interlobular interstitial thickening reflects infiltration and thickening of the interstitial framework of the secondary pulmonary lobule and may be caused by pulmonary fibrosis or inflammation in the absence of fibrosis. When underlying fibrosis is present, the reticulation often appears coarse, and traction bronchiectasis and architectural distortion.

Interlobular interstitial thickening is a common finding in patients with usual interstitial pneumonia–idiopathic pulmonary fibrosis, and may be the predominant finding before honeycombing is evident. Interlobular interstitial thickening is also a common finding in patients with nonspecific interstitial pneumonitis and pulmonary disease associated with collagen vascular diseases. Interlobular interstitial thickening may also be seen in other idiopathic interstitial pneumonias, pulmonary infections, pulmonary edema, and lymphangitic carcinomatosis.

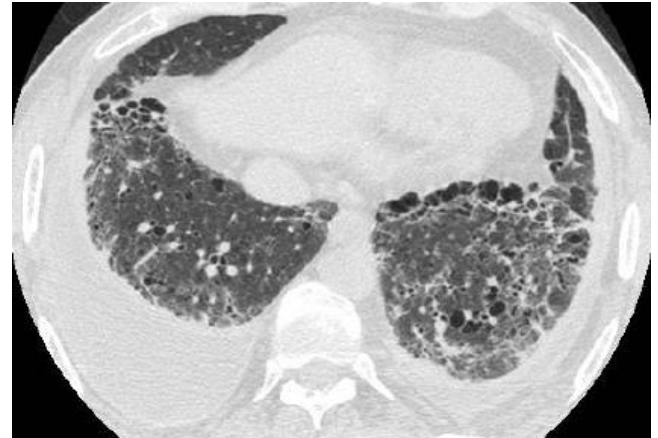


Fig 1.5 Reticulation on HRCT imaging

1.1.2 Image Processing

The field of image processing continues, as it has since the early '70s, on a path of dynamic growth in terms of popular and scientific interest and number of commercial applications. Considerable advances have been made over the past 30 years resulting in routine application of image processing to problems in medicine, manufacturing, entertainment, law enforcement, and many others. Examples include mapping internal organs in medicine using various scanning technologies (image reconstruction from projections), automatic fingerprint recognition (pattern recognition and image coding), and HDTV (video coding), to name a few. The discipline of image processing covers a vast area of scientific and engineering knowledge. It is built on a foundation of one- and two-dimensional signal processing theory and overlaps with such disciplines as artificial intelligence (scene understanding), information theory (image coding), statistical pattern recognition (image classification), communication theory (image coding and transmission), and microelectronics (image sensors, image processing hardware). Broadly, image processing may be subdivided into the following categories: enhancement, restoration, coding, and understanding. The goal in the first three categories is to improve the pictorial information either in quality (for purposes of human interpretation) or in transmission efficiency. In the last category, the objective is to obtain a symbolic description of the scene, leading to autonomous machine reasoning and perception.

Image Processing and Analysis can be defined as the "act of examining images for the purpose of identifying objects and judging their significance". A major attraction of digital imaging

is the ability to manipulate image and video information with the computer. Digital image processing is now a very important component in many industrial and commercial applications and a core component of computer vision applications. Image processing techniques also provide the basic functional support for document image analysis and many other medical applications. The field of digital image processing is continually evolving. Transform theory plays a key role in image processing. Image and signal compression is one of the most important applications of wavelets. A key idea for wavelets is the concept of "scale" The discrete wavelet transforms decomposes an image into "approximation" and "detail".

Image

The term image, refers to a two-dimensional light intensity function $f(x,y)$, where x and y denote spatial coordinates and value at any point (x, y) is proportional to the brightness of the image at that point.

Digital Image

A digital image can be considered as a matrix whose row and column indices identify a point in the image and the corresponding matrix element values identifies the gray level at that point.

In a most generalized way, a digital image is an array of numbers depicting spatial distribution of a certain field of parameters. Digital image consists of discrete picture elements called pixels.

Based on the way that image data is saved, images can be split into 3 different types:

- 1) **bitmap**
- 2) **vector**
- 3) **metafile**

Bitmap

Bitmaps images are exactly what their name says they are: a collection of bits that form an image. The image consists of a matrix of individual dots (or pixels) that all have their own color described using bits. Bitmap graphics are also called **raster images**. A picture saved using the Paint program is likely to have the .bmp file extension, for bit map. The data in .bmp files is not compressed; therefore bitmap files tend to be very large. Bitmap graphics can be saved in any of these formats: GIF, JPEG, TIFF, BMP, PICT, PNG and PCX.

Vector

In vector graphics, the co-ordinates of images (lines and curves) are saved as mathematical data. You can imagine the co-ordinates as being all the points through which lines or curves pass. It's a little like drawing a square on a piece of graph paper and describing it, using the co-ordinates of all 4 corners. Computer Aided Design (CAD) is based on vector graphics. Images produced using vector graphics are ideal for many purposes because they're so much smaller than bitmaps - it is not necessary to store information about every pixel, just about the lines and curves, their co-ordinates, width and colour.

The format of your vector graphic could be draw or one of many others depending on the software used. Examples of commercial software that uses vector graphics are Corel Draw, Macromedia Flash and Adobe Illustrator. Scalable Vector Graphics, or SVG, is a new graphics format that allows Web designers to include very realistic interactive vector graphics and animation to Web pages using only plain text commands based on XML (extensible Mark-up Language).

Metafile

Metafile graphics are simply 2D graphics that are made up of both vector and bitmap. If you drew a shape using vector graphics, and then filled it with a bitmap pattern, then you would have metafile. The vector object still retains the property of scalability without any loss of resolution. The circle above was created as a vector graphic, and then a fill added. It was saved as a .gif to include on this page, which unfortunately changes it to a bitmap with a subsequent loss of scalability.

Clip Art images for use with desktop publishing are usually supplied as metafiles. If you're a sub-editor or a desk top publishing user, you would want to be able to rescale or stretch graphics to fill the space you have, whilst retaining resolution, rather than to create one again from scratch. Metafile graphics suit this purpose admirably. The formats that you're likely to meet are: **WMF** (Windows Metafile), **EMF** (Enhanced Metafile), and **CGM** (Computer Graphics Metafile).

CGM graphics have many applications because the image size is independent of file size, which means that you can enlarge the size of the original graphic without increasing the file

size. This makes it ideal for many electronic document applications, maps (think of being able to zoom in without waiting for ages for the image to load), technical drawings, and icons.

Bitmap Graphics Formats

Bitmap graphics format is the specific format in which an image file is saved. The format is identified by three-letter extension at the end of the file name. Every format has its own characteristics, advantages and disadvantages. By defining the file format it may be possible to determine the number of bits per pixel.

Digital Image Processing

Image processing deals with the processing and display of images of real objects. Their emphasis is on the modification of the image, which takes in a digital image and produces some other information, decision etc.

A digital image is an array of real or complex processing of any two dimensional data.

1. Each point (x, y) has an intensity value, or colour
2. Not All Images Are Equal
3. Images can be manipulated to extract desired information
4. Best end results a matter of taste.

The elements of the general-purpose system capable of performing the image processing operations are

1. Image Acquisition
2. Image Storage
3. Processing the image
4. Communication
5. Display

Storage of digital processing elements falls in the following three categories. They are

1. Short-term storage - used during processing
2. Online storage - for relatively fast recall
3. Archival storage - characterized by infrequent access

Processing of digital image involves procedures that are usually expressed in algorithmic form. The exception of image acquisition and display, most image processing functions implemented in software.

Communication in digital image primarily involves local communication between image processing systems and remote processing systems and remote communication from one point to another, typically in connection with the transmission of image hardware. Communication across vast distances proposed a more serious challenge if the intent is to communicate image data rather than abstracted results.

Monochrome and color TV monitors are the principle display devices used in modern digital processing

systems. Printing image display devices are useful primarily for low-resolution image processing work.

Steps In Image Processing

The fig 1.6 shows the seven steps of digital image processing,

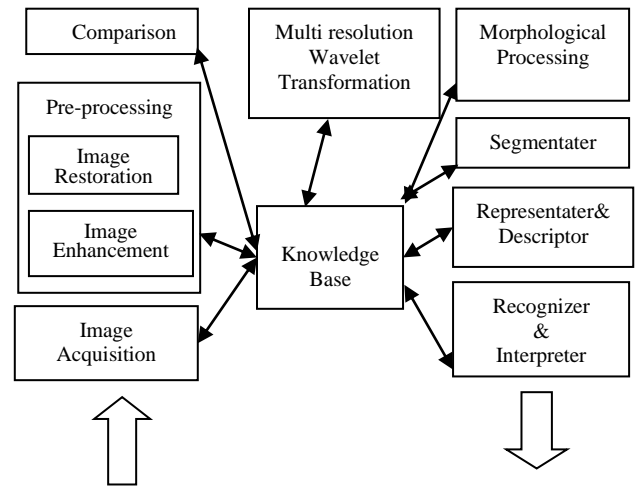


Fig 1.6 Steps involved in Image processing

Image acquisition is the process of acquiring a digital image. To acquire an image we require an imaging sensor and the capability to digitize the signal produced by the sensor

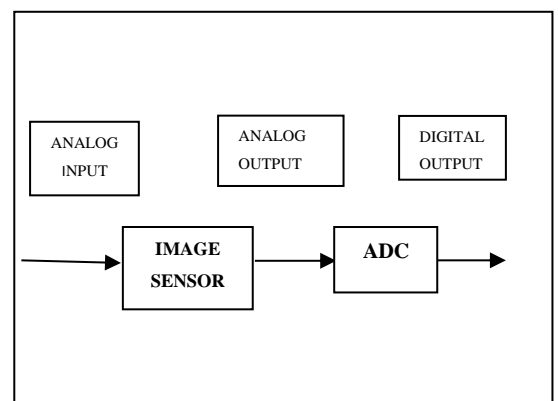


Fig 1.7 Image Acquisition

The key function of preprocessing is to improve the image in ways that increase the chances of the other process.

(i) Image enhancement

- 1) To provide more effective display of data for visual interpretation human eye can distinguish up to 40 grey shades
- 2) Increase the visual distinction between features in a scene.

- 3) "Digital darkroom" techniques
- (ii) Image rectification and restoration
- 1) Correction of geometric distortions,
 - 2) Calibration of data,
 - 3) Elimination of noise
 - 4) Correction of blurring,

Segmentation partitions the input image into its constituent parts or objects. In general, autonomous segmentation is one of the most difficult tasks in digital image processing.

Description, also called feature selection, deals with extracting features that result in some quantitative information of interest or features that are basic for differentiating one class of objects from another.

Recognition is the process that assigns a label to an object based on the information provided by its descriptors. Interpretation involves assigning meaning to an ensemble of recognized objects.

Knowledge about a problem domain is coded into an image processing system in the form of a knowledge database. This knowledge may be as simple as detailing regions of an image where the information of interest is known to be located, thus limiting the search that has to be conducted in seeking the information.

In addition to guiding the operation of each processing module, the knowledge base also controls the interaction between modules. The knowledge base guides not only the operation of each module, but it also aids in feedback operations between modules through the knowledge base

1. 2 Objective of the project

The objective of the project is to design a deep convolutional neural network (CNN) for the classification of ILD patterns.

1.3 Layout of phase report

This report is organised as follows: Chapter 2 explains literature review of the project. Chapter 3 explains project overview, description and classification methods. Chapter 4 gives detailed information about the system design implementation existing and proposed system. Chapter 5 explains about software and hardware requirements and software description. Chapter 6 shows results discussion and references of the project.

REVIEW OF LITERATURE

Near-affine-invariant texture learning for lung tissue analysis using isotropic wavelet frames, A. Depeursinge in 2012 proposed near-affine-invariant texture descriptors derived from isotropic wavelet frames for the characterization of lung tissue patterns in high-resolution computed tomography (HRCT) imaging. Affine invariance is desirable to enable learning of nondeterministic textures without a priori localizations, orientations, or sizes. When combined with complementary gray-level histograms, the proposed method

allows a global classification accuracy of 76.9% with balanced precision among five classes of lung tissue using a leave-one-patient-out cross validation, in accordance with clinical practice.

Texture-based identification and characterization of interstitial pneumonia patterns in lung multidetector CT, P. D. Korfiatis in 2009 identified and characterized the diffuse of parenchyma lung disease (DPLD) patterns challenges computer-aided schemes in computed tomography (CT) lung analysis. In this study, an automated scheme for volumetric quantification of interstitial pneumonia (IP) patterns, a subset of DPLD, is presented, utilizing a multidetector CT (MDCT) dataset. Initially, lung-field segmentation is achieved by 3-D automated gray-level thresholding combined with an edge-highlighting wavelet preprocessing step, followed by a texture-based border refinement step. The vessel tree volume is identified and removed from lung field, resulting in lung parenchyma (LP) volume. Following, identification and characterization of IP patterns is formulated as a three-class pattern classification of LP into normal, ground glass, and reticular patterns, by means of k-nearest neighbor voxel classification, exploiting 3-D cooccurrence features. Performance of the proposed scheme in identifying and characterizing ground glass and reticular patterns was evaluated by means of volume overlap (ground glass: 0.734 ± 0.057 , reticular: 0.815 ± 0.037), true-positive fraction (ground glass: 0.638 ± 0.055 , reticular: 0.942 ± 0.023) and false-positive fraction (ground glass: 0.361 ± 0.027 , reticular: 0.147 ± 0.032) on five MDCT scans.

Gradient-based learning applied to document recognition, Y. Lecun in 2002, published a paper on Multilayer neural networks trained with the back-propagation algorithm constitute the best example of a successful gradient based learning technique. Given an appropriate network architecture, gradient-based learning algorithms can be used to synthesize a complex decision surface that can classify high-dimensional patterns, such as handwritten characters, with minimal preprocessing. This paper reviews various methods applied to handwritten character recognition and compares them on a standard handwritten digit recognition task. Convolutional neural networks, which are specifically designed to deal with the variability of 2D shapes, are shown to outperform all other techniques. Real-life document recognition systems are composed of multiple modules including field extraction, segmentation recognition, and language modeling. A new

learning paradigm, called graph transformer networks (GTN), allows such multimodule systems to be trained globally using gradient-based methods so as to minimize an overall performance measure. Two systems for online handwriting recognition are described. Experiments demonstrate the advantage of global training, and the flexibility of graph transformer networks. A graph transformer network for reading a bank cheque is also described. It uses convolutional neural network character recognizers combined with global training techniques to provide record accuracy on business and personal cheques. It is deployed commercially and reads several million cheques per day.

Investigation of 3D textural features' discriminating ability in diffuse lung disease quantification in MDCT, I. Mariolis in 2010 proposed the current trend in lung CT image analysis is Computer Aided Diagnosis (CAD) schemes aiming at DLD patterns quantification. The majority of such schemes exploit textural features combined with supervised classification algorithms. In this direction, several 3D texture feature sets have been proposed. However their discriminating ability is not systematically evaluated, in terms of individual feature sets or in conjunction to different classifiers. In this paper, four classification settings combined with the RLE feature set, commonly used in the literature, and Laws feature set, first time employed for DLD characterization, are evaluated. Furthermore, the combination of RLE and Laws features was examined using the same classification settings. Although both RLE and Laws feature sets presented high discriminative ability for all classifiers considered (classification accuracy > 96.5%), their combination achieved even better results, yielding classification accuracy above 98.6%.

Lung image patch classification with automatic feature learning Qing Li, in 2013 identified that image patch classification is an important task in many different medical imaging applications. The classification performance is usually highly dependent on the effectiveness of image feature vectors. While many feature descriptors have been proposed over the past years, they can be quite complicated and domain-specific. Automatic feature learning from image data has thus emerged as a different trend recently, to capture the intrinsic image features without manual feature design. In this paper, we propose to create multi-scale feature extractors based on an unsupervised learning algorithm; and obtain the image feature vectors by convolving the feature extractors with the image patches. The auto-generated image features are data-adaptive and highly descriptive. A simple classification scheme is then used to classify the image patches. The proposed method is generic in nature and can be applied to different imaging domains. For evaluation, we perform image patch classification to differentiate various

lung tissue patterns commonly seen in interstitial lung disease (ILD), and demonstrate promising results.

Computer analysis of computed tomography scans of the lung: A survey by I.Sluimer in 2006 about the current computed tomography (CT) technology allows for near isotropic, submillimeter resolution acquisition of the complete chest in a single breath hold. These thin-slice chest scans have become indispensable in thoracic radiology, but have also substantially increased the data load for radiologists. Automating the analysis of such data is, therefore, a necessity and this has created a rapidly developing research area in medical imaging. This paper presents a review of the literature on computer analysis of the lungs in CT scans and addresses segmentation of various pulmonary structures, registration of chest scans, and applications aimed at detection, classification and quantification of chest abnormalities. In addition, research trends and challenges are identified and directions for future research are discussed.

Feature-based image patch approximation for lung tissue classification Author: Y.Song in 2013, in this paper, he proposed a new classification method for five categories of lung tissues in high-resolution computed tomography (HRCT) images, with feature-based image patch approximation. We design two new feature descriptors for higher feature descriptiveness, namely the rotation-invariant Gabor-local binary patterns (RGLBP) texture descriptor and multi-coordinate histogram of oriented gradients (MCHOG) gradient descriptor. Together with intensity features, each image patch is then labeled based on its feature approximation from reference image patches. And a new patch-adaptive sparse approximation (PASA) method is designed with the following main components: minimum discrepancy criteria for sparse-based classification, patch-specific adaptation for discriminative approximation, and feature-space weighting for distance computation. The patch-wise labelings are then accumulated as probabilistic estimations for region-level classification. The proposed method is evaluated on a publicly available ILD database, showing encouraging performance improvements over the state-of-the-arts.

Quantitative analysis of pulmonary emphysema using local binary patterns S. B. Shaker in 2010, this paper aim at improving quantitative measures of emphysema in computed tomography (CT) images of the lungs. Current standard measures, such as the relative area of emphysema (RA), rely on a single intensity threshold on individual pixels, thus ignoring any interrelations between pixels. Texture analysis allows for a much richer representation that also takes the local structure around pixels into account. This paper presents a texture classification-based system for emphysema quantification in CT images. Measures of emphysema severity are obtained by fusing pixel posterior probabilities output by a classifier. Local binary patterns (LBP) are used as texture features, and joint LBP and intensity histograms are used for characterizing regions of interest (ROIs). Classification is then performed using a k nearest neighbour classifier with a histogram dissimilarity measure as distance. A 95.2% classification accuracy was achieved on a set of 168 manually annotated ROIs, comprising the three classes: normal tissue, centrilobular emphysema, and Para septal emphysema. The measured emphysema severity was in good agreement with a pulmonary function test (PFT) achieving correlation coefficients of up to $|r| = 0.79$ in 39 subjects. The results were compared to RA and to a Gaussian filter bank, and the texture-based measures correlated significantly better with PFT than did RA.

Multiple kernel learning for classification of diffuse lung disease using HRCT lung images K.T.Vo in 2010, a novel algorithm is presented for classification of four patterns of diffuse lung disease: normal, emphysema, honeycombing and ground glass opacity, on the basis of textural analysis of high resolution computed tomography (HRCT) lung images. The algorithm incorporates scale-space features based on Gaussian derivative filters and multi-dimensional multi-scale features based on wavelet and contour let transforms of the original images. The mean, standard deviation, skewness and kurtosis along with generalized Gaussian density are used to model the output of filters and transforms, and construct feature vectors. Multi-class multiple kernel learning (m-MKL) classifier is used to evaluate the performance of the feature extraction scheme. The method is tested on a collection of 89 slices from 38 patients, each slice of size 512×512 , 16 bits/pixel in DICOM format. The dataset contains 70,000 ROIs from slices already marked by experienced radiologists. The average sensitivity and specificity achieved is 94.16% and 98.68%, respectively.

High resolution multidetector CT-aided tissue analysis and quantification of lung fibrosis V. A. Zavaletta in 2007, this study reveals the volumetric high-resolution scans can be acquired of the lungs with multidetector CT (MDCT). Such scans have potential to facilitate useful visualization, characterization, and quantification of the extent of diffuse lung diseases, such as

usual interstitial pneumonitis or idiopathic pulmonary fibrosis (UIP/IPF). There is a need to objectify, standardize, and improve the accuracy and repeatability of pulmonary disease characterization and quantification from such scans. This article presents a novel texture analysis approach toward classification and quantification of various pathologies present in lungs with UIP/IPF. The approach integrates a texture matching method with histogram feature analysis.

CHAPTER 3 METHODOLOGY

3.1 System Implementation

In this section, first describe the dataset used in the study, followed by the proposed CNN. The definition of the input data and desired outputs prior to the actual methods provides a better definition of the problem and thus a better understanding of the methods.

3.1.1 Data

The dataset used for training and evaluating the proposed method was made using two databases of ILD CT scans from two different Swiss university hospitals:

The first is the publicly available multimedia database of ILDs from the University Hospital of Geneva which consists of 109 HRCT scans of different ILD cases with pixels per slice. Manual annotations for 17 different lung patterns are also provided, along with clinical parameters from patients with histologically proven diagnoses of ILDs.

The second database was provided by the Bern University Hospital, “Inselspital”, and consists of 26 HRCT scans of ILD cases with resolution. The scans were produced by different CT scanners with slightly different pixel spacing so a pre-processing step was applied, which rescaled all scans to match a specific spacing value (i.e., 0.4 mm). However, the use of different reconstruction kernels by the scanners, still remains an open issue that complicates the problem even further. The image intensity values were cropped within the window $[-1000, 200]$ in HU and mapped. Experienced radiologists from the “Inselspital” annotated (or re-annotated) both databases by manually drawing polygons around the six most relevant ILD patterns, namely GGO, reticulation, consolidation, micro nodules, honeycombing and a combination of GGO and

reticulation. Healthy tissue was also added, leading to 7 classes.

The annotation focused on typical instances of the considered ILD patterns, excluding ambiguous tissue areas that even experienced radiologists find difficult to classify. Hence, tissue outside the polygons may belong to any pattern, including that considered. Moreover, the annotators tried to avoid the bronchovascular tree which (in a complete CAD system) should be segmented and removed.

The considered classes appeared in the annotations of 94 out of the 109 scans of the Geneva database, to which the 26 cases from “InselSpital” were added, giving a total of 120 cases. On the basis of the ground truth polygons of these cases, we extracted in total 14696 non-overlapping image patches of size 32x32, unequally distributed across the 7 classes. The number of ground truth polygons, the average and standard deviation of their area, the number of cases in which it was annotated and the number of extracted patches. The healthy pattern was only annotated in 8 cases, which however proved to be enough, since its texture does not present large deviations.

The patches are entirely included in the lung field and have an overlap with the ground truth polygons of at least 80%. For each class, 150 patches were randomly selected for the test and 150 for the validation set. The choice of 150 was made based on the patch number of the rarest class (i.e., honeycombing) leaving about 50% of the patches for training. On the remaining patches, data augmentation was employed in order to maximize the number of training samples and equalize, at the same time, the samples' distribution across the classes. Data augmentation has often been employed in image classification, in order to increase the amount of training data and prevent over-fitting. To this end, 15 label-preserving transformations were used, such as flip and rotation, as well as the combinations of the two. For each class, the necessary number of augmented samples was randomly selected, so all classes would reach the training set size of the rarest class, i.e., 5008, leading to 35056 equally distributed training patches.

3.2 Existing System

In existing system, propose a new classification method for five categories of lung tissues in high-resolution computed tomography (HRCT) images, with feature-based image patch approximation. We design two new feature descriptors for higher feature descriptiveness, namely the rotation-invariant Gabor-local binary patterns (RGLBP) texture descriptor and multi-coordinate histogram of oriented gradients (MCHOG) gradient descriptor. Together with intensity features, each image patch is then labelled based on its feature approximation from reference image patches. And a new patch-adaptive sparse approximation (PASA) method is designed with the following main components: minimum discrepancy criteria for sparse-based classification, patch-specific adaptation for discriminative approximation, and feature-space weighting for distance computation. The patch-wise labelings are then accumulated as probabilistic estimations for region-level classification.

3.2.1 Disadvantages of existing system

- It is difficult and less accuracy.
- Complexity and lack of tissue classification.
- Assessment of the tissue type is not achieved effectively.
- High computational demands.
- Higher misclassification.
- Problems of texture recognition

3.3 Proposed System

In this project, a deep CNN for the classification of ILD patterns that exploits the outstanding descriptive capability of deep neural networks. The method has been evaluated on a dataset of 120 cases from two hospitals and the results confirm its superiority compared to the state of the art. To the best of our knowledge, this is the first time a deep CNN has been designed and trained for lung tissue characterization. Finally, empirical rules and principles on the design of CNN architectures for similar texture classification problems were provided.

● PHASE I

A deep CNN is used to classify lung CT image into 7 classes, including 6 different ILD patterns and healthy tissue. A novel network architecture was designed that captures the low-level textural features of the lung tissue. Here, micro-structures that characterize texture with relatively small size, compared to whole region. The network consists of 5 convolutional layers with 2x2 kernels and LeakyReLU activations. It followed by just one average pooling, with size equal to the size of final feature maps and three dense layers. The training was performed by minimizing the categorical cross entropy with the Adam optimizer. Classification achieved using CNNs in analyzing lung patterns.

● PHASE II (THESIS)

Here, the **CLASSIFICATION** is main the process to get the final output of the image patches that was easily gives the information about the lung disease pattenen respectively.

➤ Initially the regions of interest were described by a set of texture LTCoP attributes

extracted using Lacunarity and classical methods of statistical texture analysis.

➤ Then the LNDP which are calculated based on the gray values of centre pixel and its surrounding neighbours. This approach gave promising results, outperforming the previous work on a very challenging dataset. This method can be easily trained on additional textural lung patterns while performance could be improved. ANN were employed to distinguish between lung patterns.

3.3.1 Convolution Neural Networks

CNNs are feed-forward ANN inspired by biological processes and designed to recognize patterns directly from pixel images (or other signals), by incorporating both feature extraction and classification. A typical CNN involves four types of layers: convolutional, activation, pooling and fully-connected (or dense) layers. A convolutional layer is characterized by sparse local connectivity and weight sharing. Each neuron of the layer is only connected to a small local area of the input, which resemble the receptive field in the human visual system. Different neurons respond to different local areas of the input, which overlap with each other to obtain a better representation of the image. In addition, the neurons of a convolutional layer are grouped in feature maps sharing the same weights, so the entire procedure becomes equivalent to convolution, with the shared weights being the filters for each map. Weight sharing drastically reduces the number of parameters of the network and hence increases efficiency and prevents overfitting. Convolutional layers are often followed by a non-linear activation layer, in order to capture more complex properties of the input signal. Pooling layers are also used to subsample the previous layer, by aggregating small rectangular subsets of values. Max or average pooling is usually applied by replacing the input values with the maximum or the average value, respectively. The pooling layers reduce the sensitivity of the output to small input shifts. Finally, one or more dense layers are put in place, each followed by an activation layer, which produce the classification result. The training of CNNs is performed similarly to that of other ANNs, by minimizing a loss function using gradient descent based methods and back propagation of the error.

Although the concept of CNNs has existed for decades, training such deep networks with multiple stacked layers was achieved only recently. This is mainly due to their extensive parallelization properties, which have been coupled with massively parallel GPUs, the huge amounts of available data, and several design tricks, such as the rectified linear activation units (ReLU). The proposed deep CNN, also known as AlexNet, consists of five convolutional layers with ReLU activations, some of which are followed by max-pooling layers, and three dense layers with a final 1000-way softmax. The network was trained with stochastic gradient descent (SGD) with a momentum term, maximizing the multinomial logistic regression objective. Deep architectures permit learning of data representations in multiple levels of

semantic abstraction, so even high-level visual structures like cars or faces can be recognized in the last layers by combining low-level features of the first, such as edges. Nevertheless, designing a deep CNN for a specific problem is not trivial, since a large number of mutually dependent parameter values and algorithmic choices have to be chosen. Although much research has been conducted in recent years on deep CNNs for color image classification, very little has been done on the problems of texture recognition and medical image analysis.

3.3.2 Proposed CNN

In order to decide on the optimal architecture and configuration of a CNN, one should first comprehend the nature of the problem considered in this case the classification of ILD patterns. Unlike arbitrary objects in color images, which involve complex, high-level structures with specific orientation, ILD patterns in CT images are characterized by local textural features. Although texture is an intuitively easy concept for humans to perceive, formulating a formal definition is not trivial, which is the reason for the many available definitions in the literature. Here, we define texture as a stochastic repetition of a few structures (textons) with relatively small size, compared to the whole region. Image convolution highlights small structures that resemble the convolution kernel throughout an image region, and in this way the analysis of filter bank responses has been successfully used in many texture analysis applications.

This encourages the use of CNNs to recognize texture by identifying the optimal eproblem-specific kernels; however some key aspects stemming from our definition of texture have to be considered: (i) The total receptive field of each convolutional neuron with respect to the input (i.e., the total area of the original input “seen” by a convolutional neuron) should not be larger than the characteristic local structures of texture, otherwise non-local information will be captured, which is irrelevant to the specific texture, (ii) since texture is characterized by fine grained low-level features, no pooling should be carried out between the convolutional layers, in order to prevent loss of information, (iii) each feature map outputted by the last convolutional layer should result in one single feature after pooling, in order to gain some invariance to spatial transformations like flip and rotation. Unlike color pictures that usually have high-level geometrical structure (e.g., the sky is up), a texture patch should still be a valid sample of the same class when flipped or rotated.

3.3.3 Architecture

On the basis of these principles, we designed the network presented in Fig. 3.1 the input of the network is a 32x32 image patch, which is convolved by a series of 5 convolutional layers. The size of the kernels in each layer was chosen to be minimal. The use of small kernels that lead to very deep networks was proposed in the VGG-ne which was ranked at the top of ILSVRC 2014 challenge by employing 3x3 kernels and up to 16 convolutional layers. Each layer has a number of kernels proportional to the receptive field of its neurons, so it can handle the increasing complexity of the described structures.

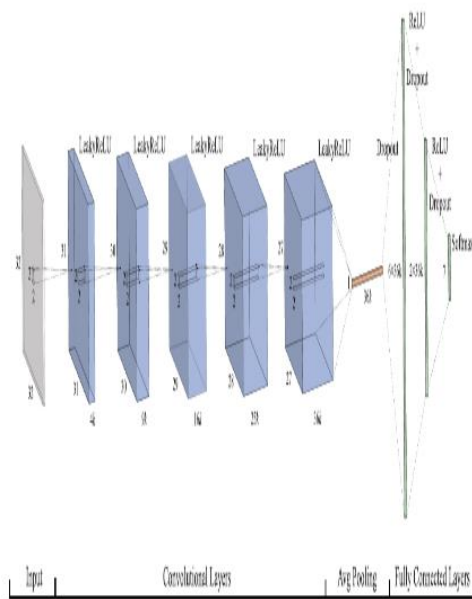


Fig 3.1 Architecture of the proposed CNN

The size of the rectangular receptive field is 2x2 for the first layer and is increased by 1 in each dimension, for each layer added, leading to an area of for the layer. Hence, the number of kernels we use for the layer is , where the parameter depends on the complexity of the input data and was set to 4 after relevant experiments. An average pooling layer follows, with size equal to the output of the last convolutional layer. The resulting features, which are equal to the number of features maps of the last layer i.e., , are fed to a series of 3 dense layers with sizes , and 7, since 7 is the number of classes considered. The use of large dense layers accelerated convergence, while the problem of overfitting was solved by adding a dropout layer before each dense layer. Dropout can be seen as a form of bagging; it randomly sets a fraction of units to 0, at each training update, and thus prevents hidden units from relying on specific inputs.

3.3.4 Activations

It is well-known that the choice of the activation function significantly affects the speed of convergence. The use of the ReLU function has been proven to speed up the training process many times compared to the classic sigmoid alternative. In this study, we also noticed that convolutional activations have a strong influence on the descriptive ability of the network. Driven by this observation and after experimenting with different rectified activations, we propose the use of LeakyReLU a variant of ReLU, for activating every convolutional layer. Unlike ReLU, which totally suppresses negative values, leaky ReLU assigns a non-zero slope, thus allowing a small gradient when the unit is not active

$$f(x) = \begin{cases} x, & x > 0 \\ ax, & \text{else} \end{cases}$$

Where a is a manually set coefficient. LeakyReLU was proposed as a solution to the “dying ReLU” problem, i.e., the tendency of ReLU to keep a neuron constantly inactive as may happen after a large gradient update. Although a very low negative slope coefficient (i.e., a) was originally proposed, here we increase its value to 0.3, which considerably improves performance. Similar observations have also been reported in other studies. A very leaky ReLU seemsto be more resilient to overfitting when applied to convolutional layers, although the exact mechanism causing this behavior has to be further studied. For the dense part of the network, the standard ReLU activation was used for the first two layers and softmax on the last layer, to squash the 7-dimensional output into a categorical probability distribution.

3.3.5 Training Method

The training of an ANN can be viewed as a combination of two components, a loss function or training objective, and an optimization algorithm that minimizes this function. Adam is a first-order gradient-based algorithm, designed for the optimization of stochastic objective functions with adaptive weight updates based on lower-order moments. Three parameters are associated with Adam: one is the learning rate and the other two are exponential decay rates for the moving averages of the gradient and the squared gradient. After relevant experiments, we left the parameters to their default values namely, learning rate equal to 0.001 and the rest 0.9 and 0.999, respectively. The initialization of the convolutional layers was performed using orthogonal matrices multiplied with a scaling parameter equal to 1.1, while a

uniform distribution was utilized for the dense layers, scaled by a factor proportional to the square root of the layer's number of inputs. The training ends when the network does not significantly improve its performance on the validation set for a predefined number of epochs. This number is set to 200 and the performance is assessed in terms of average f-score () over the different classes ((2)). An improvement is considered significant if the relative increase in performance is at least 0.5%.

3.3.6 Advantages of proposed system.

- Easier and higher accuracy.
- Limited computational resources.
- Minimize classification error
- It provides a much better efficiency
- Relative increase in performance

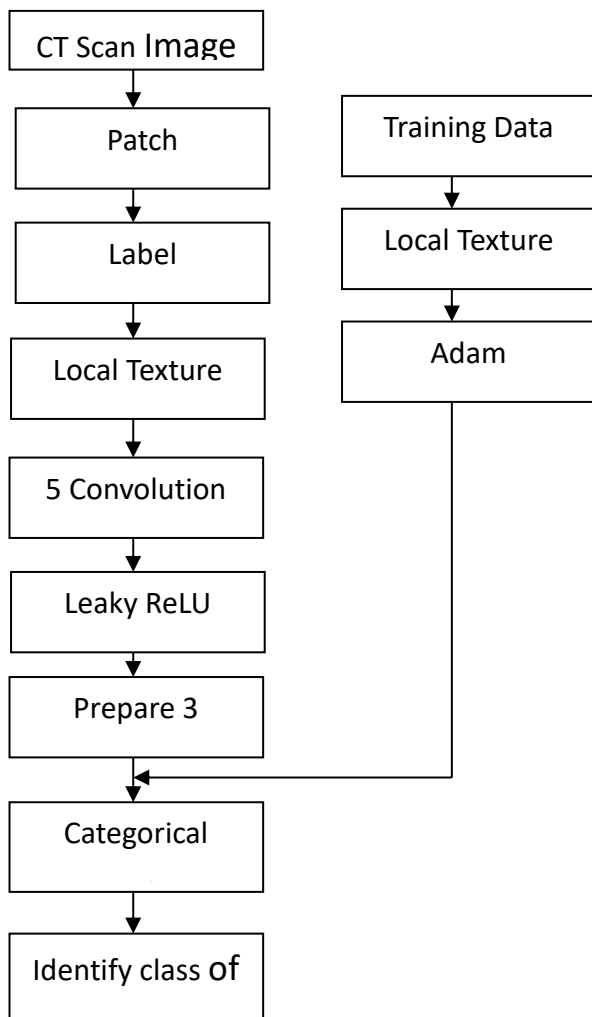


Fig. 3.2 System Architecture

3.4 System Architecture

Fig. 3.2 shows the system architecture of proposed system. Initially the CT images is get back and the patches

was selected by technician and feature extraction was done. Then by using some software like Leaky ReLU function the dense layers was prepared and training algorithm was applied. Finally, the problem was identified and treated.

Block Description

Lung pattern classification is composed of the following

- Patch Selection Module
- Local Textural Features Module
- Prepare convolution layer
- ReLU Activations
- Classification

3.4.1 Patch Selection Module

For each lung pattern, number of patches are extracted of size 32 x 32. The patches are entirely included in the lung field and have an overlap with the ground truth polygons. For each class, 20-50 patches were randomly selected for the test and 20-50 for the validation set. Data augmentation is employed to increase the amount of training data and prevent over-fitting. For each class, necessary number of augmented samples was randomly selected to increase training patches.

3.4.2 Local Textural Features Module

This system designed that captures the low-level textural features of the lung tissue. Here, define texture as a stochastic repetition of a few structures (textons) with relatively small size. In our proposed system the Texton structure map extraction process is a three step process Divide the original image into 3x3 blocks Move the 3x3 block horizontally and vertically from left to right and top to bottom throughout the original image Generate the final texton structure map using fusion of texton structure.

3.4.3 Prepare convolution layer

Use of CNNs to recognize texture by identifying the optimal problem-specific kernels. The texton structure map is convolved by a series of 5 convolutional layers. The size of the kernels in each layer was chosen to be minimal, i.e., 2x2. Here, go one step further by shrinking the kernel

size even more to 6x6. The resulting features, which are equal to the number of features maps of the last layer. Dropout can be seen as a form of bagging to prevent hidden units from relying on specific inputs.

3.4.4 ReLU Activations

It is well-known that the choice of the activation function significantly affects the speed of convergence. The use of the ReLU function has been proven to speed up the training process. Here, convolutional activations with different rectified activations, propose the use of LeakyReLU. ReLU to keep a neuron constantly inactive as may happen after a large gradient update. It is resilient to overfitting when applied to convolutional layers although exact mechanism causing this behaviour.

3.4.5 Classification

For the dense part of the network, the standard ReLU activation was used for the first two layers. Then, softmax on last layer, to squash the 7 dimensional output into a categorical probability distribution. The training of an ANN use the Adam optimizer to minimize the categorical cross entropy. Cross entropy represents the dissimilarity of approximated output distribution from the true distribution of labels. Deep CNN to classify image patches into 7 classes, including 6 different ILD patterns and healthy tissue.

computation and visualization. The combination of analysis capabilities, flexibility, reliability, and powerful graphics makes MATLAB the premier software package for scientific researchers. MATLAB provides an interactive environment with hundreds of reliable and accurate built-in mathematical functions. These functions provide solutions to a broad range of mathematical problems including matrix algebra, complex arithmetic, linear systems, differential equations, signal processing, optimization, nonlinear systems, and many other types of scientific computations. The most important feature of MATLAB is its programming capability, which is very easy to learn and to use, and which allows user-developed functions. It also allows access to FORTRAN algorithms and C codes by means of external interfaces. There are several optional toolboxes written for special applications such as signal processing, control systems design, system identification, statistics, neural networks, fuzzy logic, symbolic computations, and others. MATLAB has been enhanced by the very powerful Simulink program.

Simulink is a software package for modelling, simulating, and analyzing dynamical systems. It supports linear and nonlinear systems, modelled in continuous time, sampled time, or a hybrid of the two. Systems can also be multi-rate, i.e., have different parts that are sampled or updated at different rates. For modeling, Simulink provides a graphical user interface (GUI) for building models as block diagrams, using click-and-drag mouse operations. With this interface, you can draw the models just as you would with pencil and paper (or as most textbooks depict them). Simulink includes a comprehensive block library of sinks, sources, linear and nonlinear components, and connectors. You can also customize and create your own blocks. Models are hierarchical. This approach provides insight into how a model is organized and how its parts interact. After you define a model, you can simulate it, using a choice of integration methods, either from the Simulink menus or by entering commands in MATLAB's command window. The menus are particularly convenient for interactive work, while the command-line approach is very useful for running a batch of simulations (for example, if you are doing Monte Carlo simulations or want to sweep a parameter across a range of values). Using scopes and other display blocks, you can see the simulation results while the simulation is running. In addition, you can change parameters and immediately see what happens, for "what if" exploration. The simulation results can be put in the MATLAB workspace for post

SYSTEM REQUIREMENT

4.1 System Specification

4.1.1 Hardware Specification

Processor	: Intel Pentium D
Mother Board	: Intel 945G Express Chipset
Bus Speed	: 2.80 GHZ
RAM	: 2 GB
Hard disk	: 20 GB or more
Monitor	: 17 "inch CRT (IBM)
Keyboard	: 104 Keys
Mouse	: Lenovo PS/2
CD-ROM	: LITE-ON CD-ROM

4.1.2 Software Requirements

Operating System:	Windows 7
Front End	: MATLABR2013A

4.1.3 System Description

MATLAB

The environment in which we build our simulation model was MATLAB. The name MATLAB stands for matrix laboratory. MATLAB, developed by MathWorks Inc., is a software package for high performance numerical

processing and visualization. And because MATLAB and Simulink are integrated, you can simulate, analyze, and revise your models in either environment at any point.

Features

A family of add-on application-specific solutions called toolboxes. Very important to most users of MATLAB, toolboxes allow you to learn and apply specialized technology. Toolboxes are comprehensive collections of MATLAB functions (M-files) that extend the MATLAB environment to solve particular classes of problems. Areas in which toolboxes are available include signal processing, control systems, neural networks, fuzzy logic, wavelets, simulation, and many others.

Main Parts of MATLAB Development Environment

This is the set of tools and facilities that help you use MATLAB functions and files. Many of these tools are graphical user interfaces. It includes the MATLAB desktop and Command Window, a command history, an editor and debugger, and browsers for viewing help, the workspace, files, and the search path. The MATLAB Mathematical Function Library.

This is a vast collection of computational algorithms ranging from elementary functions like sum, sine, cosine, and complex arithmetic, to more sophisticated functions like matrix inverse, matrix eigen values, Bessel functions, and fast Fourier transforms.

The MATLAB Language

This is a high-level matrix/array language with control flow statements, functions, data structures, input/output, and object-oriented programming features. It allows both "programming in the small" to rapidly create quick and dirty throw-away programs, and "programming in the large" to create complete large and complex application programs.

Graphics

MATLAB has extensive facilities for displaying vectors and matrices as graphs, as well as annotating and printing these graphs. It includes high-level functions for two-dimensional and three-dimensional data visualization, image processing, animation, and proposedation graphics.

It also includes low-level functions that allow you to fully customize the appearance of graphics as well as to build complete graphical user interfaces on your MATLAB applications.

The MATLAB application program interface (API)

This is a library that allows you to write C and FORTRAN programs that interact with MATLAB. It includes facilities for calling routines from MATLAB (dynamic linking), calling MATLAB as a computational engine, and for reading And Writing MAT-Files.

Functions

Displaying images with 'IMSHOW'

In MATLAB, the primary way to display images is by using the image function. This function creates a Handle Graphics image object, and it includes syntax for setting the various properties of the object. MATLAB also includes the 'imagesc' function, which is similar to image but which automatically scales the input data.

The Image Processing Toolbox includes an additional display routine called 'imshow'. Like image and 'imagesc', this function creates a Handle Graphics image object. However, 'imshow' also automatically sets various Handle Graphics properties and attributes of the image to optimize the display.

In general, using 'imshow' for image processing applications is preferable to using image and 'imagesc'.

Subplot

Create and control multiple axes.

Syntax

Subplot(m,n,p)

Subplot (m,n,p,'replace')

Subplot (m,n,p,'align')

Subplot(h)

Subplot ('Position', [left bottom width height])

h=subplot...)

Description

Subplot divides the current figure into rectangular panes that are numbered row wise. Each pane contains an axes. Subsequent plots are output to the current pane. 'Subplot (m,n,p)' creates an axes in the pth pane of a figure divided into an m-by-n matrix of rectangular panes. The new axes becomes the current axes. If p is a vector, it specifies and axes having a position that covers all the subplot positions listed in p.

Figure

Create figure window.

'FIGURE', by itself, creates a new figure window, and returns its handle. Figure creates figure graphics objects. Figure objects are the

individual windows on the screen in which MATLAB displays graphical output. Figure creates a new figure object using default property values.

Imread

Read image from graphics file.

A = 'IMREAD (FILENAME, FMT)' reads a grayscale or color image from the file specified by the string FILENAME, where the string FMT specifies the format of the file. See the reference page, or the output of the function 'IMFORMATS', for a list of supported formats. If the file is not in the current directory or in a directory in the MATLAB path, specify the full pathname of the location on your system. If 'IMREAD' cannot find a file name FILENAME, it looks for a file named FILENAME.FMT.

'IMREAD' returns the image data in the array A. If the file contains array scale image, A is a two-dimensional (M-by-N) array. If the file contains a color image, A is a three-dimensional (M-by-N-by-e) array. The class of the returned array depends on the data type used by the file format.

For most file formats, the color image data returned uses the RGBcolor space. For TIFF files, however, 'IMREAD' can return color data that uses the RGB, CIELAB, ICCLAB, or CYMK color spaces. If the color image uses the CYMK color space, A is an M-by-N-by-4 array. [X,MAP] = IMREAD (FILENAME,FMT) reads the indexed image in FILENAME into X and its associated colormap into MAP. Colormap values in the image file are automatically rescaled into the range [0,1]

5.1 RESULTS

Input Image

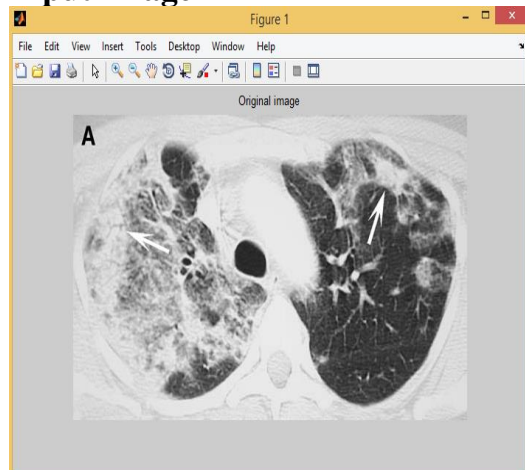


Fig. 5.1 Input Image

Here Fig.5.1 shows the raw lung input image which can be get back from CT Images from various hospitals. To train and evaluate the CNN, we used a dataset of 1469 image patches, derived by 20 CT scans from different scanners and hospitals. To the best of our knowledge, this is the first deep CNN designed for the specific problem.

Region of Interest (ROI)

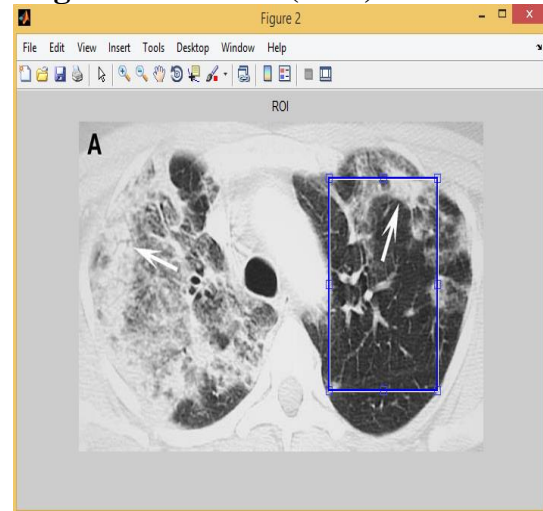


Fig. 5.2 Region of Interest (ROI)

Then the region where the technicians want to detect the abnormality in lung was marked. That can be shown in fig.5.2.

Selected Region

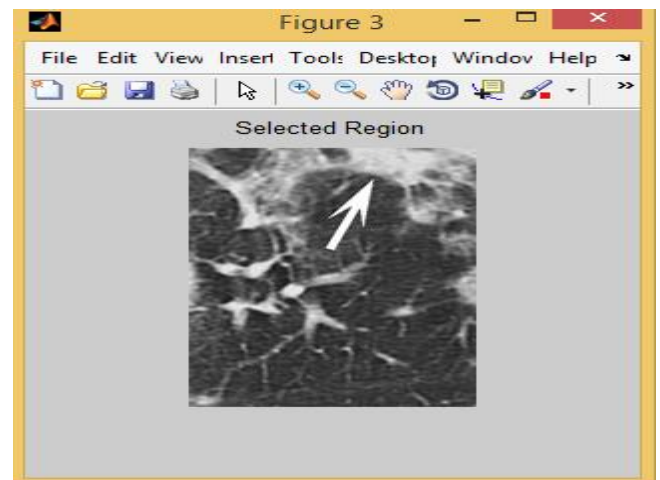


Fig. 5.3 Selected Region

Then the selected region is separately shown in fig.5.3 and that was clearly noted by the technician.

Patch Selection

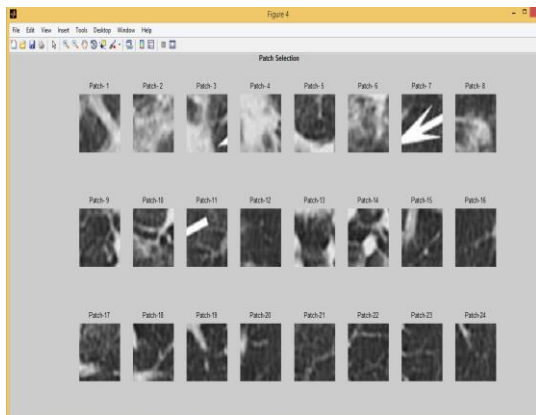


Fig. 5.4 Patch Selection

Next the patches was appeared in different pattern of the selected region that was shown in fig.5.4. For each lung pattern, number of patches are extracted of size 32 x 32. The patches are entirely included in the lung field and have an overlap with the ground truth polygons. For each class, 20-50 patches were randomly selected for the test and 20-50 for the validation set. Data augmentation is employed to increase the amount of training data and prevent over-fitting. For each class, necessary number of augmented samples was randomly selected to increase training patches.

Texton Structure Map

The fig.5.5 shows the texton structure map for the selected region of the lung. This system designed that captures the low-level textural features of the lung tissue.

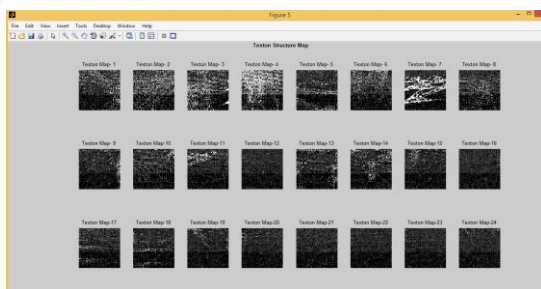


Fig. 5.5 Texton Structure Map

Here, define texture as a stochastic repetition of a few structures (textons) with relatively small size. In our proposed system the Texton structure map extraction process is a three step process Divide the original image into 3x3 blocks Move the 3x3 block horizontally and vertically from left to right and top to bottom throughout the original image Generate the final texton structure map using fusion of texton structure.

CLASSIFICATION

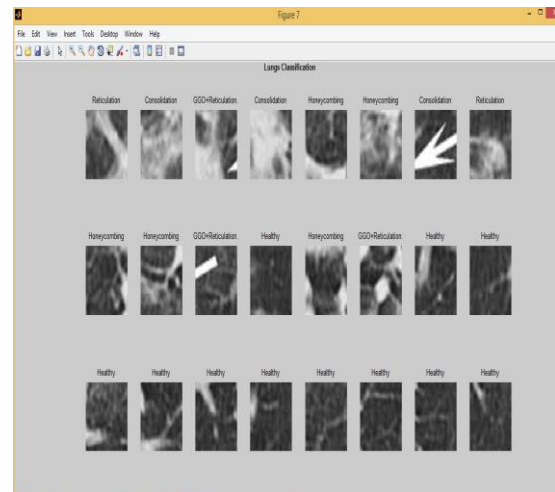


Fig 5.6 Classification

Finally from this figure the lung pattern classified and shows the diseases pattern respectively. For the dense part of the network, the standard ReLU activation was used for the first two layers. Then, softmax on last layer, to squash the 7 dimensional output into a categorical probability distribution. The training of an ANN use the Adam optimizer to minimize the categorical cross entropy. Cross entropy represents the dissimilarity of approximated output distribution from the true distribution of labels. Deep CNN to classify image patches into 7 classes, including 6 different ILD patterns and healthy tissue.

5.2 DISCUSSION

The evaluation of the different ILD patch classification approaches is based on a train-validation-test scheme. The actual training of the methods was carried-out on the training set, while the validation set was used for fine tune the hyper-parameters; the overall performance of each system was assessed on the test set. As principle evaluation measure and the average F-score over the different classes due to its increased sensitivity to imbalances among the classes; the overall accuracy is also computed. It has to be noted that the presented performances are not comparable to performances reported in the literature due to the use of different datasets and the consideration of different patterns. However, trust that the difficulty of a dataset may only affect the absolute performance of methods and not their relative performance rank.

$$F_{avg} = \frac{2}{7} \sum_{c=1}^7 \frac{recall\ c * precision\ c}{recall\ c + precision\ c}$$

$$\text{Recall}_c = \frac{\text{samples correctly classified as } c}{\text{samples classified as } c}$$

$$\text{Precision}_c = \frac{\text{samples correctly classified as } c}{\text{samples classified as } c}$$

$$\text{Accuracy} = \frac{\text{correctly classified samples}}{\text{total number of samples}}$$

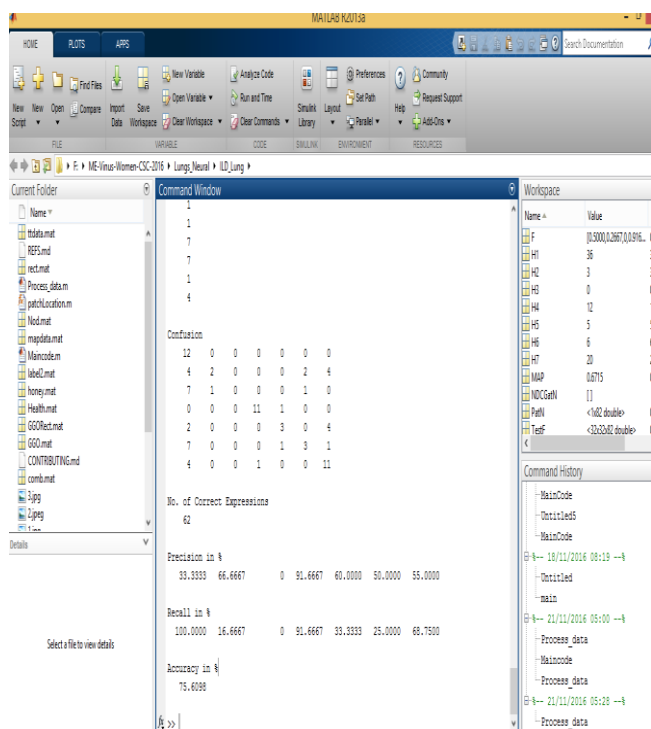


Fig 5.7 Performance Evaluation

This figure shows the overall performance of the image patches; they are, precision, recall and accuracy.

6.1 CONCLUSION

In this project, proposed a deep CNN to classify lung CT image patches into 7 classes, including 6 different ILD patterns and healthy tissue. A novel network architecture was designed that captures the low-level textural features of the lung tissue. The network consists of 5 convolutional layers with 2x2 kernels and LeakyReLU activations, followed by just one average pooling, with size equal to the size of final feature maps and three dense layers. The training was performed by minimizing the categorical cross entropy with the Adam optimizer. The proposed approach gave promising results, outperforming the state of the art on a very challenging dataset of 120 CT scans from different hospitals and scanners. The method can be easily trained on additional textural lung patterns while performance could be further improved by a more extensive investigation of the involved parameters. The large number of parameters and the relatively slow training (typically a few hours) could be considered as a

drawback of this kind of DL approaches, together with the slight fluctuation of the results, for the same input, due to the random initialization of the weights.

6.2 FUTURE WORK

In future work, regions of interest were described by a set of texture LTCoP attributes extracted using Lacunarity and classical methods of statistical texture analysis. The LTCoP encodes the co-occurrence of similar ternary edges which are calculated based on the gray values of center pixel and its surrounding neighbors. This approach gave promising results, outperforming the previous work on a very challenging dataset. This method can be easily trained on additional textural lung patterns while performance could be improved. Hybrid kernel Support Vector Machines were employed to distinguish between lung patterns.

REFERENCES

- Jin, C., Mao, X., Liu, Y., & Xie, Y. (2020). Interstitial lung disease classification using a residual convolutional neural network. *BMC medical imaging*, 20(1), 1-11.
- Wang, J., Li, F., Li, R., Li, Q., & Zhang, M. (2020). Interstitial lung disease classification based on 3D convolutional neural networks. *Biomedical Signal Processing and Control*, 56, 101771.
- Zhang, W., Zhou, Y., Liu, J., Gao, Y., & Shen, D. (2020). Interstitial lung disease classification using a 3D deep convolutional neural network with multiple feature fusion. *IEEE Transactions on Cybernetics*, 50(7), 3009-3018.
- Gao, Y., Lu, L., Harrison, A. P., Xie, Y., & Shen, D. (2019). Interstitial lung disease pattern classification using a deep convolutional neural network. *Journal of Computer Assisted Tomography*, 43(1), 98-103.
- Li, Q., Li, H., Li, R., Wang, X., & Zhang, M. (2019). Interstitial lung disease classification using multi-objective deep learning. *Computerized Medical Imaging and Graphics*, 78, 101658.
- Raghavendra, U., Fujita, H., Bhandary, S. V., & Iyengar, S. S. (2017). Deep convolutional neural network for the automated diagnosis of congestive heart

- failure using ECG signals. *Computers in biology and medicine*, 89, 18-25.
7. Yu, L., Zhang, Y., Lu, L., & Chen, H. (2017). Automatic multi-label classification of lung diseases using radiomic features. *Medical physics*, 44(2), 564- 575.
 8. M. Anthimopoulos, S. Christodoulidis, A. Christe, and S. Mouggiakakou, "Classification of interstitial lung disease patterns using local DCT features and random forest," in Proc. 36th Annu. Int. Conf. IEEE Eng. Med. Biol. Soc., 2014, pp. 6040–6043
 9. Y. Song, W. Cai, Y. Zhou, and D. D. Feng, "Feature-based image patch approximation for lung tissue classification," *IEEE Trans. Med. Imag.*, vol. 32, no. 4, pp. 797–808, Apr. 2013.
 - 10.
 11. [10]. I. Sluimer, A. Schilham, M. Prokop, and B. Van Ginneken, "Computer analysis of computed tomography scans of the lung: A survey," *IEEE Trans. Med. Imag.*, vol. 25, no. 4, pp. 385–405, Apr. 2006.
 12. Y. Uchiyama et al., "Quantitative computerized analysis of diffuse lung disease in high-resolution computed tomography," *Med. Phys.*, vol. 30, no. 9, pp. 2440–2454, 2003.
 13. L. Sørensen, S. B. Shaker, and M. De Bruijne, "Quantitative analysis of pulmonary emphysema using local binary patterns," *IEEE Trans. Med. Imag.*, vol. 29, no. 2, pp. 559–569, Feb. 2010.
 14. K. T. Vo and A. Sowmya, "Multiple kernel learning for classification of diffuse lung disease using HRCT lung images," in Proc. IEEE Eng. Med. Biol. Soc. Conf., 2010, vol. 2010, pp. 3085–3088.
 15. Y. Xu et al., "Computer-aided classification of interstitial lung diseases via MDCT: 3D adaptive multiple feature method (3D AMFM)," *Acad. Radiol.*, vol. 13, no. 8, pp. 969–978, 2006.
 16. V. A. Zavaletta, B. J. Bartholmai, and R. A. Robb, "High resolution multidetector CT-aided tissue analysis and quantification of lung fibrosis," *Acad. Radiol.*, vol. 14, no. 7, pp. 772–787, 2007.